scientific **data**

Check for updates

DATA DESCRIPTOR

Foot kinematics and kinetics data for different static foot posture collected using a multi-segment foot model

Enrique Sanchis-Sales[1]✉, Joaquín L. Sancho-Bru[2], Alba Roda-Sales[2], MaJosé Chiva-Miralles[1] & Carmen García-Gomáriz[1]

This dataset presents human foot joints kinematics and kinetics data during walking, classified by static foot posture, filling a gap in existing lower limb databases that lack data on foot joints beyond the ankle or on static posture data, despite its link to foot and lower limb pathologies. Kinematics were recorded using a three-dimensional mocap system, and kinetics through a pressure platform, employing a multi-segment foot model including the ankle, midtarsal and first metatarsophalangeal joint. The dataset contains 350 recordings of right foot joint angles and moments and contact pressures from 70 healthy subjects with varying static posture (highly pronated, highly supinated and normal). Data were collected at 100 Hz, filtered and resampled to 100 frames throughout the stance phase. Descriptive data are also provided: age, weight, height, BMI and foot anthropometric data and foot posture index. Plots, tables and ANOVAs are included for validation. Presented in .xlsx and .mat formats, this database can assist professionals in corrective footwear design, insole customization, surgical planning, and evaluating interventions on foot dynamics.

Background & Summary

The foot, a complex system with numerous degrees of freedom (DOF), facilitates various weightbearing activities like walking, running, jumping, climbing, or descending stairs. Abnormal motion and forces on foot joints during these activities can lead to pathologies such as patellar tendinopathy, Iliotibial band friction syndrome, or plantar fascitis[1]. The static foot posture (pronated, normal, or supinated) has been linked to lower limb injuries, and studying foot joint dynamics during gait aids in understanding injury development[2]. Several kinematics and kinetics databases exist for the lower limb[3–9]. The main differences among these databases lie in the activities analyzed (walking[5,6,8,9], stair ascent and descent[6,7], and obstacle negotiation[7]), in the systems used to measure kinematics (IMUs[4,5,7,9] or camera-based motion capture systems[3,6,8]), and in the kinetic data included (joint moments[3,6], EMG[3,4,6]). However, none include foot joint information (beyond the ankle). Moreover, these databases do not provide data representative of different static foot postures.

The investigation of foot kinematics is crucial for characterizing healthy movement patterns[10], evaluating patients with pathologies[11–13], and advancing foot orthoses development[14,15]. However, kinetic studies focusing on joint moments in foot joints have been limited due to challenges in segmenting forces within foot segments[16–18]. Existing databases typically exclude information on foot joints beyond the ankle, as the foot is often treated as a rigid segment, although a few multi-segment foot models have been proposed[19–23]. Therefore, it is essential to provide databases that include both kinematics and kinetics information on foot joints using these multi-segment foot models, enabling more comprehensive investigation.

The authors previously investigated foot joint dynamics using a modified multi-segment model proposed by Bruening[21], finding variations in rotations, moments, and dynamic stiffness across different static foot postures measured with the foot posture index (FPI)[10,16,24]. The FPI is a test described and validated by Redmond[25], that allows feet to be classified into 5 groups based on 6 items. It assesses the position of the foot in 3D and has been

[1]Departmental Section of Podiatry, Nursing Department, Universitat de València, 46010, Valencia, Spain. [2]Department of Mechanical Engineering and Construction, Universitat Jaume I, 12071, Castelló, Spain. ✉e-mail: enrique.sanchis-sales@uv.es
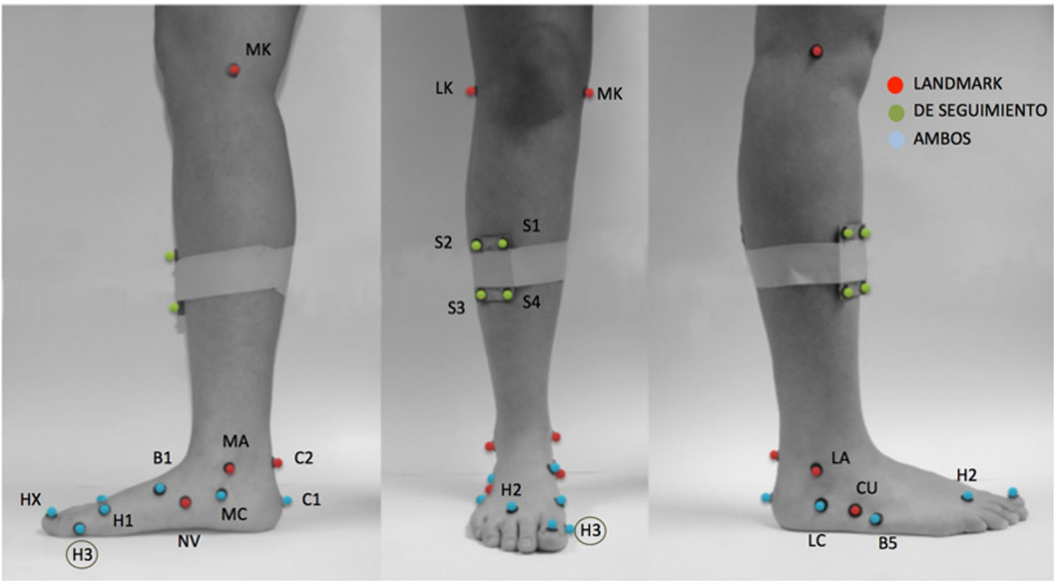
Fig. 1 Markers required for foot kinematics recording using an infra-red camera system and considering the multi-segment foot model proposed in Sanchis-Sales et al.[24]. Anatomical location described in Table 1.

MARKER	DENOMINATION	ANATOMICAL LOCATION
LK	Lateral knee	Apex of the lateral epicondyle of the femur
MK	Medial knee	Apex of the medial epicondyle of the femur
S1-S4	Shank shell	Metal plate on the shank with 4 markers
LA	Lateral ankle	Apex of the lateral malleolus
MA	Medial ankle	Apex of the medial malleolus
C1	Calcaneus 1	Apex of the calcaneal prominence
C2	Calcaneus 2	Apex of the second calcaneal prominence
LC	Lateral calcaneus	Lateral calcaneus
MC	Medial calcaneus	Medial calcaneus
NV	Navicular	Medial prominence of the navicular bone
CU	Cuboid	Center of the lateral of the cuboid bone
B1	Base 1	Lateral of the base of the first metatarsal
B5	Base 5	Lateral of the base of the fifth metatarsal
H1	Head 1	Upper prominence of the head of the first metatarsal
H2	Head 2	Between upper prominences of the head of the second and third metatarsals
H3	Hallux 3	Lateral prominence of the second metatarsophalangeal joint of the toe.
HX	Hallux	Center of the toenail of the big toe.
Virtual landmarks		
KJC	Knee joint center	Midpoint between LK and MK
AJC	Ankle joint center (without correction)	Midpoint between LA and MA
ACC	Ankle complex center (joint between shank and rearfoot)	A line is drawn between KJC and AJC, and extended inferiorly a 2.7% of shank length (distance between KJC and AJC)
MTC	Midtarsal joint center (joint between rearfoot and forefoot)	Midpoint between CU and NV
MPC	1st metatarsophalangeal joint center (joint between forefoot and hallux)	Projecting H1 vertically and considering half of the distance from H1 to the floor
FF_Dist	Forefoot distal end	Projecting H2 vertically and considering half of the distance from H2 to the floor
HxX_Dist	Hallux distal end	Projecting HX vertically and considering half of the distance from HX to the floor

Table 1. Anatomical location of the markers described in Fig. 1 and description of the virtual landmarks derived from them.

used for different purposes, such as investigating the relationship between foot types and injuries in athletes[26], the association between foot types and falls in the elderly[27] or the relationship between foot type and risk of ulceration in diabetic patients[28], among others. Pronated feet showed less range of motion (ROM) than normal or supinated feet during propulsion, greater moments in the midtarsal and first metatarsophalangeal joints than

SEGMENT	LONG AXIS	PLANE	TRACKING MARKERS
Shank	KJC to ACC	KJC, LA, MA (coronal)	S1-S4
Rearfoot	C1 to MTC	C1, MTC, C2 (sagittal)	C1, LC, MC
Forefoot	MTC to FF_Dist	MTC, FF_Dist, H2 (sagittal)	B1, B5, H2
Hallux	MPC to HX_Dist	MPC, HX_Dist, H1 (sagittal)	HX, H1, H3

Table 2. Segment reference frames are defined by a long (primary) axis, and a plane. The secondary axis is perpendicular to the plane, and the tertiary axis is perpendicular to both the primary and secondary axes. All reference frames align with the body planes in the static pose. The position and orientation of the segment is tracked using a set of tracking markers.

Fig. 2 View of the distribution of the 8 Vicon cameras and the location of the pressure platform in the middle of the walkway.

supinated feet, and higher dynamic stiffness during propulsion compared to normal or supinated feet[16]. Despite the observed differences in kinematic and kinetic behavior among feet with different static postures, databases categorized by FPI are lacking.

This article presents a dataset comprising 350 recordings of 3D anatomical angles and joint moments of the ankle, midtarsal, and first metatarsophalangeal joints of the right foot during the stance phase of walking, the right foot contact pressures recorded and basic participants' data (age, weight, height, and foot anthropometric data and foot posture index for both feet). The experiments involved 70 healthy male participants, selected so as to represent the adult population, controlling for age and foot type. The presented data adhere to ISB sign conventions[29]. Hence, the novelty of this dataset is twofold: (i) providing kinematics and kinetics data of foot joints obtained using a multi-segment foot model, and (ii) categorizing these data by FPI. This dataset can be utilized in various practical applications, such as enhancing the design of orthotic devices and footwear by providing detailed insights into the biomechanics of different foot types. It can also aid in the development of more accurate and individualized rehabilitation protocols for individuals recovering from foot injuries by analyzing joint movements and pressure distributions specific to different foot postures. Additionally, the dataset offers a valuable resource for researchers interested in studying the relationship between foot morphology and gait, potentially leading to improved diagnostic tools for identifying and managing conditions like flatfoot or high arch. This data, categorized by FPI, enables targeted studies that can ultimately lead to more effective interventions.

CRITERIA	SCORE
FPI_1: Bulge in the region of talonavicular joint (TNJ)	If area of TNJ is markedly concave, FPI_1 = −2 If area of TNJ is slightly, but definitely concave, FPI_1 = −1 If area of TNJ is flat, FPI_1 = 0 If area of TNJ is bulging slightly, FPI_1 = 1 If area of TNJ is bulging markedly, FPI_1 = 2
FPI_2: Curves above and below lateral malleoli	If curves are straight or convex, FPI_1 = −2 If the curve below is concave, but flatter/shallower than the curve above, FPI_1 = −1 If curves are roughly equal, FPI_1 = 0 If the curve below is more concave than the curve above, FPI_1 = 1 If the curve below is markedly more concave than the curve above, FPI_1 = 2
FPI_3: Congruence of the medial longitudinal arch (MLA)	If MLA is high and acutely angled towards its posterior end, FPI_1 = −2 If MLA is moderately high and slightly acute posteriorly, FPI_1 = −1 If MLA has normal height and is concentrically curved, FPI_1 = 0 If MLA is lowered with some flattening in the central portion, FPI_1 = 1 If MLA is very low with severe flattening in the central portion making ground contact, FPI_1 = 2
FPI_4: Talar head (TH) palpation	If TH is palpable on lateral side/but not on medial side, FPI_1 = −2 If TH is palpable on lateral side/slightly palpable on medial side, FPI_1 = −1 If TH is equally palpable on lateral and medial side, FPI_1 = 0 If TH is slightly palpable on lateral side/palpable on medial side, FPI_1 = 1 If TH is not palpable on lateral side/but palpable on medial side, FPI_1 = 2
FPI_5: Calcaneal position in the frontal plane (CPF)	If CPF is more than an estimated 5° inverted (varus), FPI_1 = −2 If CPF is between vertical and an estimated 5° inverted (varus), FPI_1 = −1 If CPF is perpendicular to the ground, FPI_1 = 0 If CPF is between vertical and an estimated 5° everted (valgus), FPI_1 = 1 If CPF is more than an estimated 5° everted (valgus), FPI_1 = 2
FPI_6: Abduction/adduction of the forefoot on the rearfoot	If no lateral toes are visible and medial toes are clearly visible, FPI_1 = −2 If medial toes are clearly more visible than lateral, FPI_1 = −1 If medial and lateral toes are equally visible, FPI_1 = 0 If lateral toes are clearly more visible than medial, FPI_1 = 1 If no medial toes are visible and lateral toes clearly visible, FPI_1 = 2

Table 3. Detail of the items provided in the FPI.

Methods

Study participants. The study included 70 male participants with an average age of 28 ± 7 years. Their average weight was 79.05 ± 14.34 kg, height 179.26 ± 7.04 cm, and BMI 24.7 kg/m². To be eligible for the study, participants had to be men between the ages of 18 and 60, with no lower limb pathologies, no diabetes, and no history of foot or ankle surgery. Participants were categorized based on their Foot Posture Index (FPI) into normal, highly pronated, and highly supinated groups[25]. Using the software G*Power 3.1[30], it was estimated that a sample size of 20 subjects per group (30 in normal foot group) and three groups, with a large effect size of 0.4 and a significance level of 0.05, would achieve a statistical power of 77.6%, which is close to the recommended 80%[31].

Before participating in the study, all individuals provided informed consent. The experiments were conducted in compliance with the Ethics Committee of Universitat Jaume I (approval number CD/UJI/03/12/2013). The participants' informed consent included permission to use and share the collected data for scientific purposes, and the researchers committed to ensuring that the identities of the participants will remain confidential at all times.

Acquisition protocol. *Kinematics acquisition.* Foot kinematics were captured using an adapted multi-segment foot model as in previous studies[16,24,32], based on the model introduced by Bruening *et al.*[21]. This model necessitates recording kinematics utilizing 20 markers, which include both landmarks and tracking markers (Fig. 1), which correspond to bony prominences that are easy to palpate. The markers (Vicon reflective 9.5 mm spherical pearl hard markers) were attached to the skin at specific anatomical points (Table 1) with double-sided tape by an experienced podiatrist with extensive knowledge of the anatomy of the lower extremity. These markers were tracked at a sampling rate of 100 Hz using an eight-camera infrared motion analysis system (Vicon Motion Systems Ltd., Oxford, UK). The 3-D coordinates of the markers were used to define the coordinate system of each segment (shank, rearfoot, forefoot, and hallux) and the joint centers (ankle, midtarsal, and 1st metatarsophalangeal joint), as outlined in Table 2. The position and orientation of the segments were tracked following the approach proposed by Söderkvist & Wedin[33]. Joint angles were computed with reference to the participant's standing static posture, employing a Cardan rotation sequence for all tracked segments: 1 - dorsiflexion/plantarflexion (DF/PF), 2 - abduction/adduction (AB/AD), and 3 - inversion/eversion (IN/EV). Lastly, all kinematic data underwent low-pass filtering using a second-order Butterworth filter with a cut-off frequency of 5 Hz, applied in a zero-phase manner using forward-backward filtering.

Kinetics acquisition. The multisegment kinetics were calculated using the same approach as in previous studies[16,24,32,34]. Contact pressures on the right foot were measured using a Podoprint pressure platform (Namrol Group, Barcelona, Spain) at a sampling rate of 100 Hz, synchronized with the infrared camera system. The spatial mapping of pressure cells to the global coordinate system was achieved during calibration by aligning the coordinate system's origin with the center of the pressure platform and matching the X and Y axes to the mediolateral and anteroposterior axes. In each frame, pressure data were segmented by comparing the Y-coordinates of the contact cells with the anteroposterior positions of the joint rotation centers at the moment when the foot was

VAR ID	VARIABLE	CONTENT
1	PARTICIPANT	Participant ID.
2	FPI_RF	Measured FPI in participant's right foot.
3	FPI_LF	Measured FPI in participant's left foot.
4	FPI_CLASSIFICATION	Classification according to measured FPI in their right foot (0 = Neutral, 1 = Highly Supinated, 2 = Highly Pronated).
5	WEIGHT	Participant weight (in kg).
6	HEIGHT	Participant height (in cm).
7	RF_LENGTH	Participant right foot length (in mm) (see Fig. 3).
8	LF_LENGTH	Participant left foot length (in mm) (see Fig. 3).
9	RF_EXT_LENGTH	Participant right foot external length (in mm) (see Fig. 3).
10	LF_EXT_LENGTH	Participant left foot external length (in mm) (see Fig. 3).
11	RF_WIDTH	Participant right foot width (in mm) (see Fig. 3).
12	LF_WIDTH	Participant left foot width (in mm) (see Fig. 3).
13	RF_ HEEL_WIDTH	Participant right foot heel width (in mm) (see Fig. 3).
14	LF_HEEL_WIDTH	Participant left foot heel width (in mm) (see Fig. 3).
15	RF_ MALLEOLUS_HEIGHT	Participant right foot malleolus height (in mm) (see Fig. 3).
16	LF_ MALLEOLUS_HEIGHT	Participant left foot malleolus height (in mm) (see Fig. 3).
17	RF_FINGER_SHAPE	Participant right foot finger shape according to Ogawa et al.[49] (1 = Egyptian, 2 = Greek, 3 = Squared).
18	LF_FINGER_SHAPE	Participant left foot finger shape according to Ogawa et al.[49] (1 = Egyptian, 2 = Greek, 3 = Squared).
19	AGE	Participant age (in years).
20	TRIAL	Number of recording (1 to 5).
21	FRAME	Frame of the stance phase (1 to 100).
22	R_ANK_AB	Ankle rotation in abduction/adduction plane (in degrees).
22	R_ANK_INV	Ankle rotation in inversion/eversion plane (in degrees).
24	R_ANK_DF	Ankle rotation in dorsiflexion/plantaflexion plane (in degrees).
25	R_MT_AB	Metatarsal joint rotation in abduction/adduction plane (in degrees).
26	R_MT_INV	Metatarsal joint rotation in inversion/eversion plane (in degrees).
27	R_MT_DF	Metatarsal joint rotation in dorsiflexion/plantaflexion plane (in degrees).
28	R_MP_AB	1st metatarsophalangeal joint rotation in abduction/adduction plane (in degrees).
29	R_MP_INV	1st metatarsophalangeal joint rotation in inversion/eversion plane (in degrees).
30	R MP_DF	1st metatarsophalangeal joint rotation in dorsiflexion/plantaflexion plane (in degrees).
31	M_ANK_AB	Ankle moment in abduction/adduction plane (in Nm/Kg).
32	M_ANK_INV	Ankle moment in inversion/eversion plane (in Nm/Kg).
33	M_ANK_DF	Ankle moment in dorsiflexion/plantaflexion plane (in Nm/Kg).
34	M_MT_AB	Metatarsal joint moment in abduction/adduction plane (in Nm/Kg).
35	M_MT_INV	Metatarsal joint moment in inversion/eversion plane (in Nm/Kg).
36	M_MT_DF	Metatarsal joint moment in dorsiflexion/plantaflexion plane (in Nm/Kg).
37	M_MP_AB	1st metatarsophalangeal joint moment in abduction/adduction plane (in Nm/Kg).
38	M_MP_INV	1st metatarsophalangeal joint moment in inversion/eversion plane (in Nm/Kg).
39	M_MP_DF	1st metatarsophalangeal joint moment in dorsiflexion/plantaflexion plane (in Nm/Kg).

Table 4. Detail of the variables provided in the excel file.

fully in contact with the platform. For instance, cells whose anteroposterior coordinates fell between those of the midtarsal and metatarsophalangeal joint centers were attributed to the forefoot segment. The normal component of the ground reaction forces and centers of pressure were determined for each foot segment, considering the area of active pressure cells. Following the model introduced by Bruening et al.[17], the 3-D joint moments were computed as the cross product of the ground reaction forces on the distal segments and the 3-D distances between the centers of pressure and the joint rotation centers. According to previous works[35–37], the effect of the weight of the foot and that of foot angular velocity and linear and angular accelerations was neglected.

Normalization and filtering. Joint moments were adjusted for body weight, consistent with the methods used in earlier research studies[4,19]. To minimize noise, joint angles and moments underwent low-pass filtering using a second-order Butterworth filter with a cut-off frequency of 5 Hz, applied in a zero-phase manner using forward-backward filtering. Subsequently, all joint angles, all moments, and all pressure data were resampled to 100 frames, evenly spaced across the stance phase for uniform analysis.

Software used. All kinematic and kinetic computations were performed using custom-developed software in Matlab version R2022b (The MathWorks Inc., Natick, MA, USA).
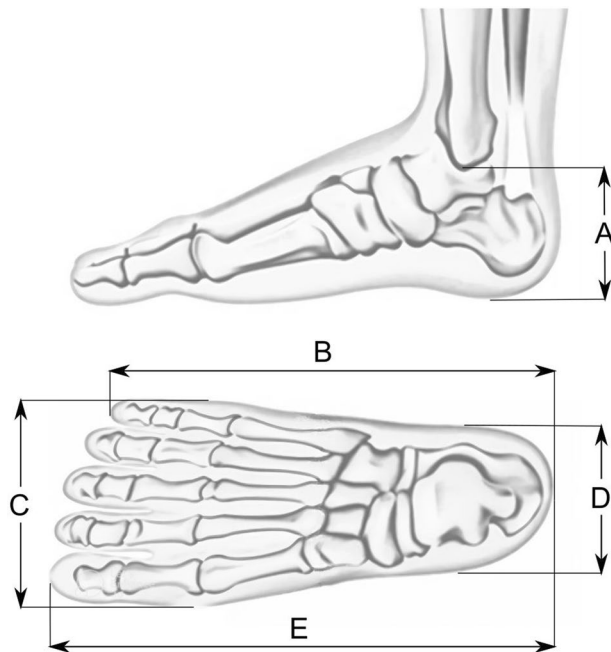
Fig. 3 Foot anthropometric measurements provided in the dataset. (**A**) (Ankle height), (**B**) (Lateral foot length), (**C**) (Forefoot width), (**D**) (Rearfoot width), (**E**) (Total foot length).

	AGE (Y)	HEIGHT (m)	WEIGHT (Kg)	BMI	FPI
NORMAL	27.13 ± 3.82	1.78 ± 0.06	78.18 ± 13.9	24.46 ± 3.57	2.27 ± 1.48
HIGHLY SUPINATED	28.55 ± 9.09	1.81 ± 0.09	78.73 ± 8.53	24 ± 1.95	-8.45 ± 1.85
HIGHLY PRONATED	29.6 ± 7.39	1.79 ± 0.07	80.68 ± 19.38	25.13 ± 5.11	10.65 ± 0.67

Table 5. Anthropometrics data of the participants in each group.

Environment. The experiments were carried out at the Biomechanics and Ergonomics research group laboratory, at Universitat Jaume I de Castelló (Spain). The setup comprised the pressure platform located in the center of the walkway, and the 8 Vicon cameras located around the walkway (Fig. 2).

Trials recorded. Before capturing foot kinematics during walking, a reference posture (the relaxed position of the calcaneus while standing) was recorded for each participant and used as the zero point for all rotational angles. To ensure natural walking patterns, participants practiced walking down the walkway multiple times prior to data collection. They were instructed to step onto the pressure platform with their right foot without directly looking at it, to avoid altering their gait. Participants repeated the task as needed until they completed five valid trials, excluding any trials where the right foot did not make contact with the platform.

FPI measurement and group classification. Foot posture index was measured according to Redmond *et al.*[25]. Participants were asked to stand barefoot on a flat surface, with their feet parallel and their weight equally distributed. Then, a trained observer stood behind the participant and performed a visual inspection from the front, back and sides of the foot, evaluating six different criteria and assigning a specific score for each one (FPI_i) (Table 3). The sum of all the scores obtained for each foot will give the result of the FPI ($FPI = SUM(FPI\_i)$), with the final score being values between -12 and $+12$. With this, the foot is classified as follows: Highly pronated: $>$ $+10$; Pronated: $+6$ to $+9$; Normal: 0 to $+5$; Supinated: -1 to -4; Highly supinated: -5 to -12.

Data Records

Data are presented as an .xlsx file (DATA.xlsx) and as Matlab structure file (DATA.mat), which contains the same information as the .xlsx file and also the contact pressure data. All the data is publicly available to all research community at the Zenodo open repository[38]. The dataset comprises variables related to participant's characteristics, 3-D rotations and moments of each studied joint and foot contact pressures. The excel file consists of 35001 rows by 39 columns. The first row contains the names of the variables, as defined in Table 4. The remaining rows contain the data for each participant, trial, and frame ($70 \times 5 \times 100 = 35000$). The Matlab file contains the data organized into a nested structure. Within this structure, the descriptive data for each participant p (variables 2 to 19 of Table 3) is organized as *PARTICIPANT(p).VARIABLE*. E.g., the weight of participant 35 can be accessed as *PARTICIPANT(35).WEIGHT*. The joint angles and moments for each participant p, for a given trial t and frame f (variables 22 to 39 in Table 3) is organized as *PARTICIPANT(p).TRIAL(t).VARIABLE(f)*.
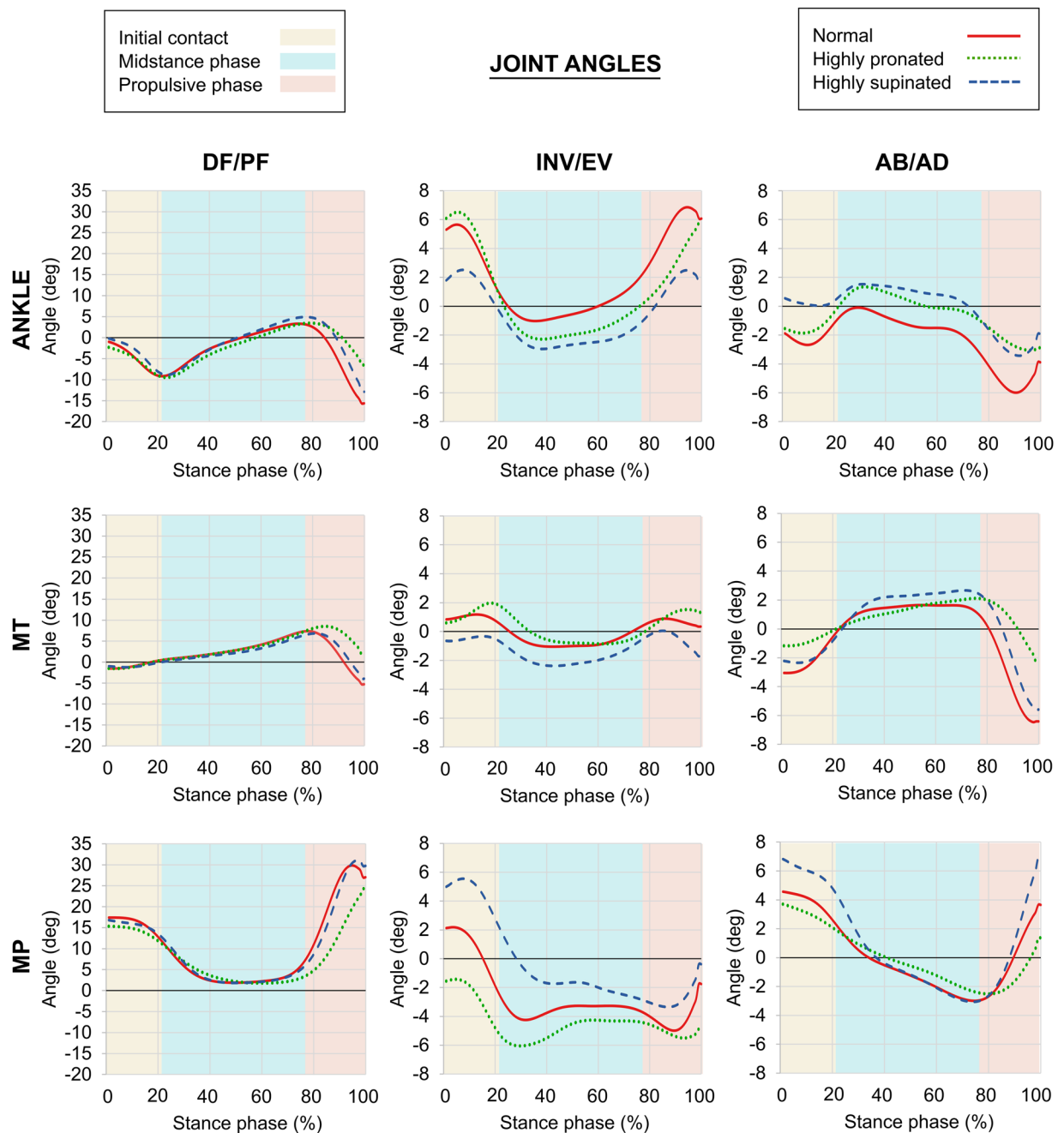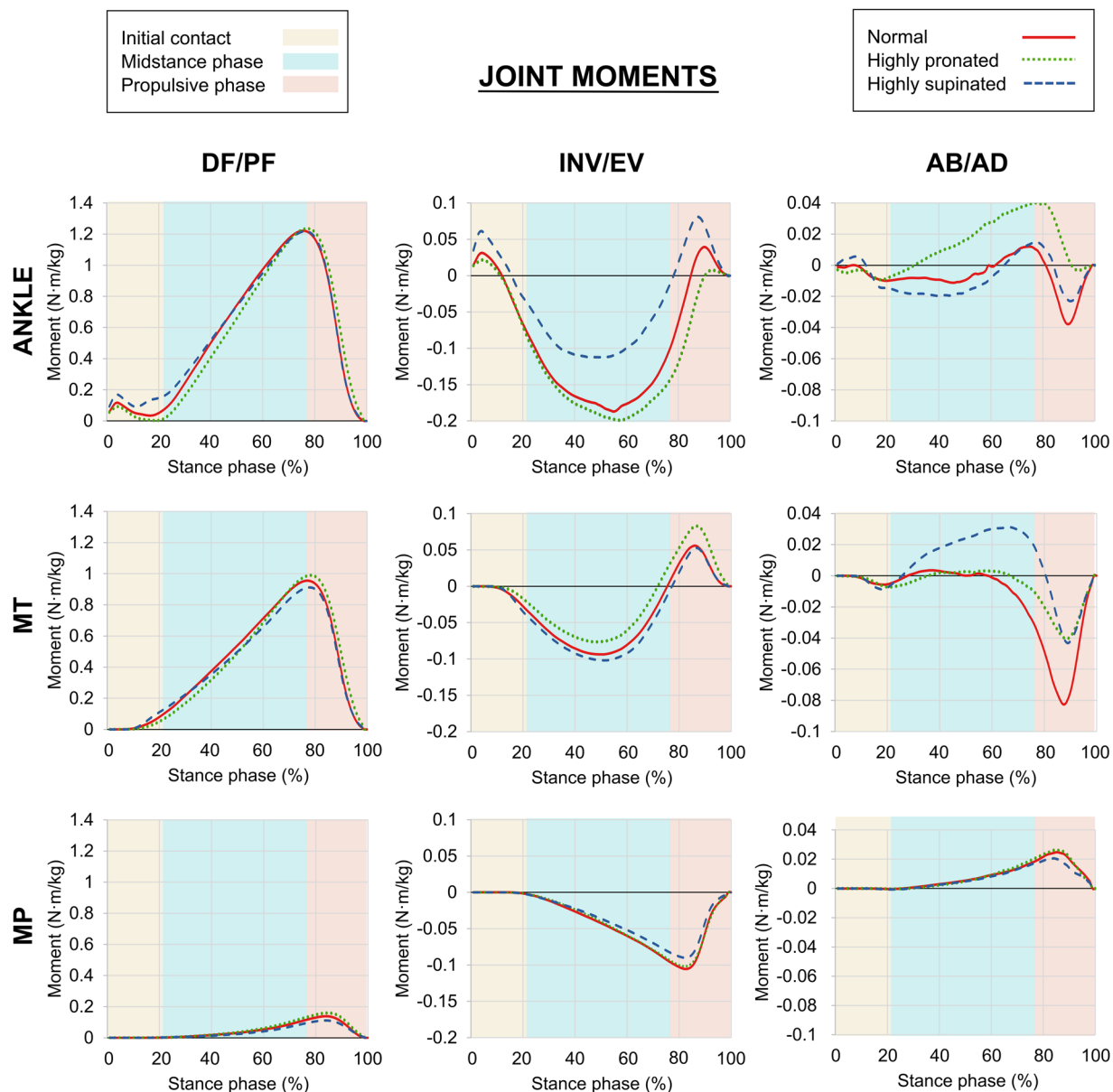
Fig. 4 Mean joint angles during all the stance phase in each joint and plane of motion, separated by foot type, with different phases of gait color-coded. Joint labelling/abbreviations: ANKLE for ankle, MT for midtarsal, MP for metatarsophalangeal. Plane of motion abbreviations: DF/PF for dorsiflexion/plantarflexion, INV/EV for inversion/eversion, AB/AD for abduction/adduction. Note that plot scale is different for DF/PF plane of motion.

E.g., the ankle joint moment in inversion/eversion plane for frame 21 of trial 4 of participant 35 can be accessed as *PARTICIPANT(35).TRIAL(4).M_ANK_INV(21)*. The Matlab structure contains two additional variables: *PRESS*, containing a 40x40x100 matrix with the pressure (in N/cm^2) in each contact cell for all frames; and PMAX, containing the maximum value of PRESS matrix. E.g., the contact pressures (a matrix 40×40) for frame 21 of trial 4 of participant 35 can be accessed as *PARTICIPANT(35).TRIAL(4).PRESS(:,:,21)*, while the maximum pressure at any contact cell during the stance phase is *PARTICIPANT(35).TRIAL(4).PMAX*.

The anthropometric measurements provided for both feet are detailed in Fig. 3.

The sign criteria considered for 3-D joint rotations and moments of the three joints was defined as follows:

- Abduction $(+)$/Adduction $(-)$
- Inversion $(+)$/Eversion $(-)$
- Dorsiflexion $(+)$/Plantarflexion $(-)$

Fig. 5 Mean joint moments during all the stance phase in each joint and plane of motion, separated by foot type, with different phases of gait color-coded. Joint labelling/abbreviations: ANKLE for ankle, MT for midtarsal, MP for metatarsophalangeal. Plane of motion abbreviations: DF/PF for dorsiflexion/plantarflexion, INV/EV for inversion/eversion, AB/AD for abduction/adduction. Note that plot scale is different for DF/PF plane of motion.

Technical Validation

Data acquisition. Before and after each trial recorded, the correct placement of the reflective markers was checked, and the pressure platform recording was revised, in order to ensure that the footprint was recorded in full. In case of not being recorded in full, the trial was repeated.

Statistical descriptive analysis of data collected. The anthropometrics data of the participants in each group are shown in Table 5. In order to validate the data, mean values across trials of joint angles and moments for each studied joint and plane of motion during the stance phase were plotted separately for each foot type group (Figs. 4, 5). Additionally, box and whisker plots of maximum and minimum joint angles and moments for each plane of motion in the three studied joints were generated, with separation by foot type group (Fig. 6). A statistical analysis was also conducted using SPSS version 28.0 (IBM Corp., Armonk, NY, USA) to identify differences in these extreme joint angles and moments between the different foot type groups. This was done by means of a set of ANOVAs with foot type as the independent factor and the extreme joint angles and moments as the dependent variables. Bonferroni post-hoc tests were then applied to determine specific group differences. Statistics of the extreme joint angles and moments, along with the results from the statistical tests are presented in Figs. 7, 8). Finally, to validate the contact pressure data provided, box and whisker plots of maximum pressure values
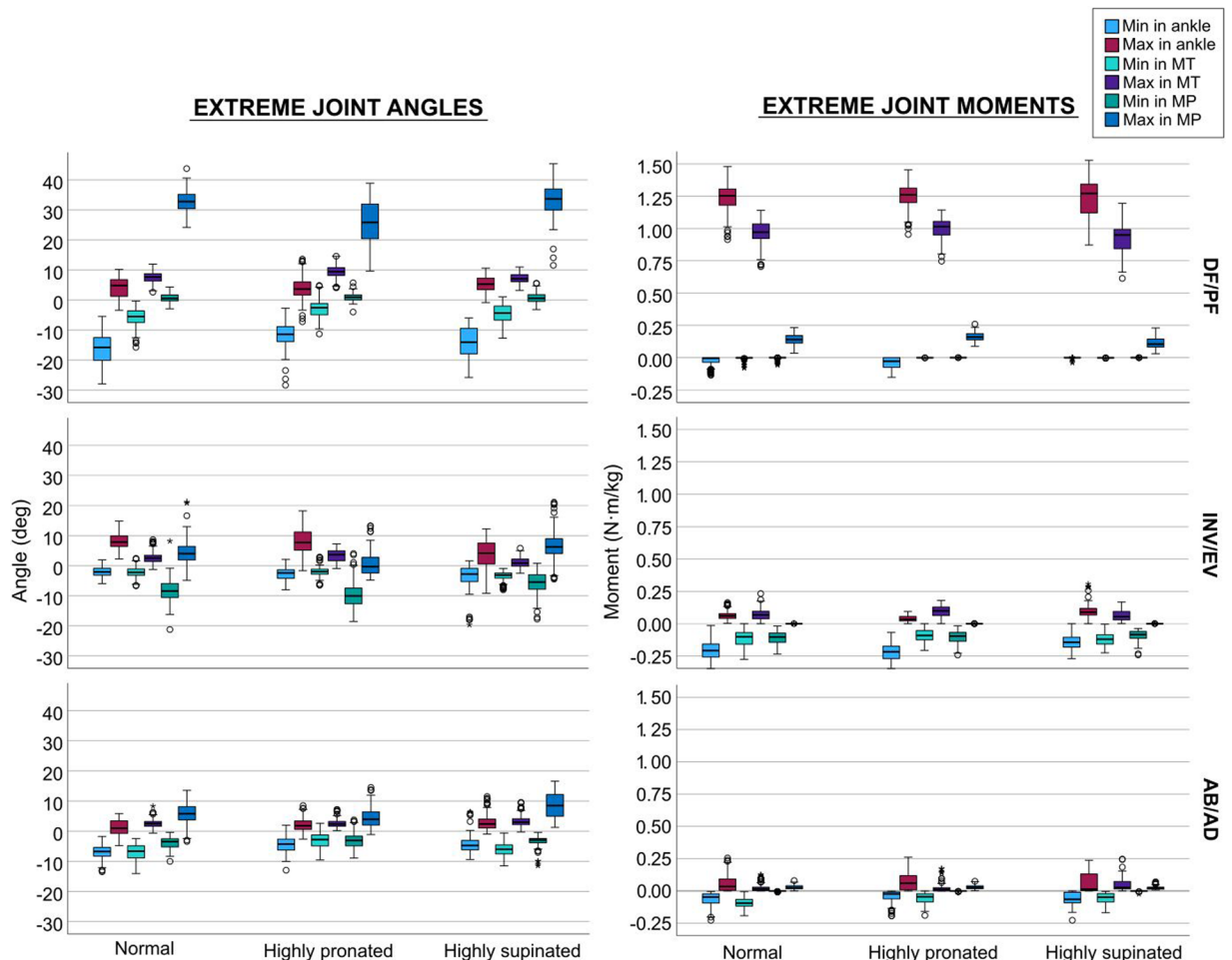
Fig. 6 Extreme joint angles and moments for each participant and trial in each joint and plane of motion, separated by foot type. Joint labelling/abbreviations: ANKLE for ankle, MT for midtarsal, MP for metatarsophalangeal. Plane of motion abbreviations: DF/PF for dorsiflexion/plantarflexion, INV/EV for inversion/eversion, AB/AD for abduction/adduction.

			Sig.	EXTREME JOINT ANGLES								
				NORMAL			HIGHLY PRONATED			HIGHLY SUPINATED		
				MEAN	SD	95% CI	MEAN	SD	95% CI	MEAN	SD	95% CI
ANKLE	DF/PF	MIN*	0.008	-16.08^P	5.05	[-16.90, -15.27]	-11.76^N	4.24	[-12.60, -10.92]	-14.30	5.53	[-15.40, -13.20]
		MAX	0.417	4.17	3.17	[3.66, 4.68]	4.00	4.11	[3.18, 4.81]	5.25	2.70	[4.71, 5.79]
	INV/EV	MIN	0.114	-2.05	1.69	[-2.33, -1.78]	-2.86	2.25	[-3.30, -2.41]	-3.73	4.32	[-4.59, -2.88]
		MAX*	<0.001	8.06^S	2.60	[7.64, 8.47]	7.94^S	4.13	[7.12, 8.76]	3.91^{N,P}	4.64	[2.99, 4.83]
	AB/AD	MIN*	<0.001	-6.83^{P,S}	2.44	[-7.22, -6.43]	-4.18^N	2.99	[-4.78, -3.59]	-4.23^N	3.09	[-4.84, -3.62]
		MAX*	0.039	1.20^S	2.51	[0.80, 1.61]	2.10	2.30	[1.65, 2.56]	3.02^N	2.77	[2.47, 3.57]
MT	DF/PF	MIN*	0.003	-5.80^P	3.01	[-6.29, -5.31]	-2.83^N	2.98	[-3.42, -2.23]	-4.77	3.10	[-5.39, -4.16]
		MAX*	<0.001	7.55^P	1.89	[7.24, 7.85]	9.44^{N,S}	2.10	[9.02, 9.85]	7.20^P	1.86	[6.83, 7.56]
	INV/EV	MIN*	0.004	-2.21^S	1.66	[-2.48, -1.94]	-1.94^S	1.64	[-2.27, -1.61]	-3.52^{N,P}	1.64	[-3.84, -3.19]
		MAX*	<0.001	2.64^S	1.74	[2.36, 2.92]	3.26^S	1.95	[2.87, 3.64]	1.07^{N,P}	1.70	[0.74, 1.41]
	AB/AD	MIN*	<0.001	-7.05^S	2.76	[-7.49, -6.60]	-2.98^{N,S}	2.61	[-3.50, -2.46]	-6.01^P	2.21	[-6.45, -5.57]
		MAX	0.060	2.47	1.36	[2.25, 2.69]	2.54	1.50	[2.25, 2.84]	3.42	1.92	[3.04, 3.80]
MP	DF/PF	MIN	0.588	0.65	1.32	[0.44, 0.86]	0.99	1.35	[0.72, 1.25]	0.59	1.78	[0.24, 0.95]
		MAX*	<0.001	32.63^P	3.79	[32.02, 33.24]	25.97^{N,S}	7.26	[24.53, 27.41]	33.03^P	6.14	[31.81, 34.25]
	INV/EV	MIN*	0.004	-8.32	3.71	[-8.91, -7.72]	-9.80^S	4.75	[-10.74, -8.86]	-5.78^P	3.64	[-6.51, -5.06]
		MAX*	<0.001	4.02^P	4.35	[3.32, 4.73]	0.71^{N,S}	4.13	[-0.11, 1.53]	6.53^P	5.53	[5.43, 7.63]
	AB/AD	MIN	0.459	-3.89	1.85	[-4.19, -3.59]	-3.20	2.52	[-3.71, -2.70]	-3.46	1.92	[-3.84, -3.08]
		MAX*	0.002	5.58^S	3.24	[5.05, 6.10]	4.51^S	3.45	[3.83, 5.20]	8.59^{N,P}	4.20	[7.76, 9.43]

Fig. 7 Statistics of the extreme joint angles, along with the results from the statistical tests. Significant differences (p < 0.05) between means are highlighted with color, and a superscript indicates the specific groups with which differences were found (P for highly pronated, S for highly supinated and N for normal).

			Sig.	EXTREME JOINT MOMENTS								
				NORMAL			HIGHLY PRONATED			HIGHLY SUPINATED		
				MEAN	SD	95% CI	MEAN	SD	95% CI	MEAN	SD	95% CI
ANKLE	DF/PF	MIN*	<0.001	-0.03^{S}	0.04	[-0.03, -0.02]	-0.04^{S}	0.04	[-0.05, -0.03]	$0.00^{N,P}$	0.01	[0.00, 0.00]
		MAX	0.813	1.24	0.10	[1.22, 1.26]	1.25	0.10	[1.23, 1.27]	1.23	0.15	[1.20, 1.26]
	INV/EV	MIN*	<0.001	-0.21^{S}	0.07	[-0.22, -0.20]	-0.22^{S}	0.06	[-0.24, -0.21]	$-0.14^{N,P}$	0.06	[-0.15, -0.13]
		MAX*	<0.001	0.06^{S}	0.03	[0.06, 0.07]	0.04^{S}	0.02	[0.03, 0.04]	$0.10^{N,P}$	0.06	[0.09, 0.11]
	AB/AD	MIN	0.221	-0.07	0.05	[-0.07, -0.06]	-0.04	0.05	[-0.05, -0.03]	-0.06	0.05	[-0.07, 0.05]
		MAX	0.485	0.05	0.06	[0.05, 0.06]	0.08	0.07	[0.06, 0.09]	0.06	0.07	[0.05, 0.08]
MT	DF/PF	MIN*	0.025	-0.01^{P}	0.01	[-0.01, 0.00]	0.00^{N}	0.00	[0.00, 0.00]	0.00	0.00	[0.00, 0.00]
		MAX*	0.018	0.97	0.09	[0.95, 0.98]	1.00	0.09	[0.98, 1.02]	0.92	0.12	[0.89, 0.94]
	INV/EV	MIN	0.245	-0.11	0.07	[-0.12, -0.10]	-0.09	0.05	[-0.11, -0.08]	-0.12	0.05	[-0.13, -0.11]
		MAX*	0.016	0.07	0.04	[0.06, 0.08]	0.09^{S}	0.05	[0.09, 0.10]	0.06^{P}	0.04	[0.06, 0.07]
	AB/AD	MIN*	<0.001	$-0.09^{S,P}$	0.04	[-0.10, -0.09]	-0.06^{N}	0.04	[-0.06, -0.05]	-0.05^{N}	0.04	[-0.06, -0.05]
		MAX*	0.035	0.02^{S}	0.03	[0.02, 0.03]	0.02	0.04	[0.02, 0.03]	0.05^{N}	0.05	[0.04, 0.06]
MP	DF/PF	MIN*	0.031	0.00	0.01	[-0.01, 0.00]	0.00	0.00	[0.00, 0.00]	0.00	0.00	[0.00, 0.00]
		MAX*	<0.001	0.14^{S}	0.04	[0.13, 0.15]	0.16^{S}	0.04	[0.16, 0.17]	$0.11^{N,P}$	0.05	[0.11, 0.12]
	INV/EV	MIN	0.462	-0.11	0.05	[-0.12, -0.10]	-0.10	0.05	[-0.11, -0.09]	-0.09	0.04	[-0.10, -0.08]
		MAX	0.880	0.00	0.00	[0.00, 0.00]	0.00	0.00	[0.00, 0.00]	0.00	0.00	[0.00, 0.00]
	AB/AD	MIN	0.506	0.00	0.00	[0.00, 0.00]	0.00	0.00	[0.00, 0.00]	0.00	0.00	[0.00, 0.00]
		MAX	0.281	0.03	0.02	[0.03, 0.03]	0.03	0.02	[0.03, 0.03]	0.02	0.01	[0.02,0.03]

Fig. 8 Statistics of the extreme joint moments, along with the results from the statistical tests. Significant differences (p < 0.05) between means are highlighted with color, and a superscript indicates the specific groups with which differences were found (P for highly pronated, S for highly supinated and N for normal).
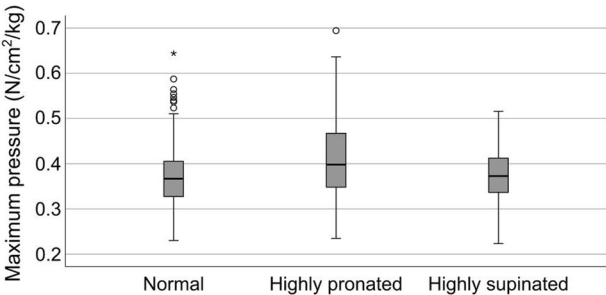

Fig. 9 Maximum normalized pressure values recorded for each participant trial separated by foot type group.

recorded for each participant trial, normalized with respect to the participant's weight, were also represented, also separated by foot type group (Fig. 9). And the contact pressures of a subject of each foot type are shown for different instances of the stance phase (Fig. 10).

The angles and moments for the ankle, midtarsal, and metatarsophalangeal joints during the stance phase (Figs. 4, 5) are consistent with the patterns observed in previous studies[39–43], showing bell-shaped profiles for dorsiflexion moments in all three joints. Peak values at the ankle and midtarsal joints occur at the beginning of the propulsion phase, coinciding with the dorsiflexion angle peaks in these joints. The extreme angles (Figs. 6, 7) are within the reported ROM of each joint[40,44,45] thus validating the presented dataset. The statistical tests identified several significant differences in the extreme joint angles between different foot posture groups, consistent with the findings reported in the literature[39,40]. For example, a significantly lower peak ankle adduction was found in supinated feet compared to normal feet[40], with a difference of 3.7°, while in our study, it was 2.6°. Similarly, the same study[40] reported a 2° higher peak dorsiflexion in the midtarsal joint of highly pronated individuals, consistent with the 2.2° observed in our data.

The moment values obtained in our study are also consistent with those reported in other studies[42,43], with the highest peak dorsiflexion moments occurring at the ankle, around 1.2 N·m/kg, close to the 1.3 N·m/kg observed in previous studies[17]. The extreme moments (Fig. 6) for both the ankle and midtarsal joints consistently fall within the expected ranges[41], reinforcing the reliability of the dataset. Again, several significant differences were found in the extreme joint moments between different foot posture groups, with individuals with highly supinated feet showing a higher inversion peak at the ankle and a higher abduction peak at the midtarsal joint. The differences in both the extreme joint angles and moments highlight the importance of providing kinematic and kinetic data differentiated by static foot posture.

Regarding plantar pressures, we found that highly pronated feet exhibit higher pressures (Fig. 9), which is consistent with previous studies that reported higher values on the medial longitudinal arch and the hallux of pronated feet compared to other feet[46]. The pressure patterns plotted in Fig. 10 also match the expected patterns for each type of foot: the normal foot exhibits a more homogeneous pattern, with highest pressure on the central
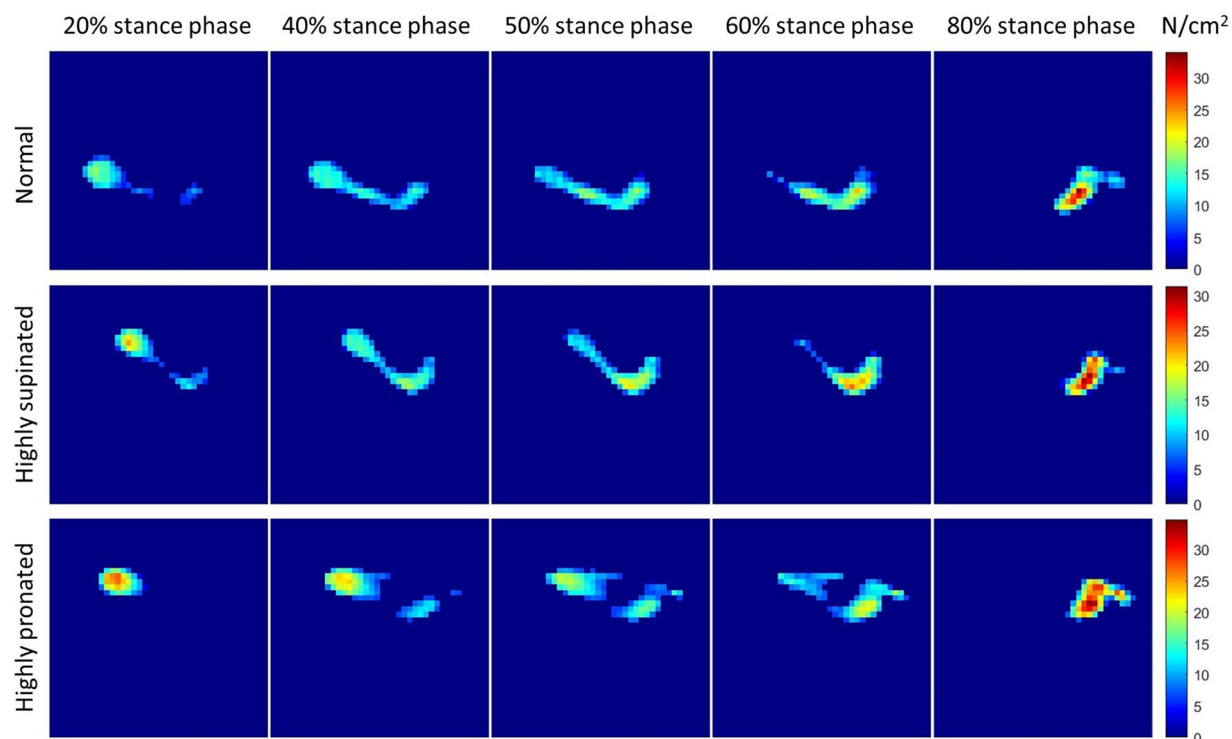
Fig. 10 Contact pressures of a subject of each foot type group for different instances of the stance phase. The normal foot data correspond to trial 3 of participant 10 (FPI = 1), the highly supinated foot to trial 3 of participant 33 (FPI = −11), and the highly pronated foot data to trial 3 of participant 60 (FPI = 12).

metatarsal heads during the propulsive phase (80% of the stance phase); the highly supinated foot exhibits elevated pressures on the external longitudinal arch during the midstance phase (50–60% of the stance phase), with highest pressure on the external metatarsal heads during the propulsive phase; and the highly pronated foot shows contact on the internal longitudinal arch from the initial midstance phase, with decreased pressures on the outer edge, as well as increased pressures on the 1st and 2nd metatarsal heads during the propulsive phase.

Usage Notes

These data can be used for several applications, such as medicine, biomechanics, biomedical engineering, and footwear design, among others. With a database containing information on the biomechanical characteristics of a patient's foot, health professional can customize treatments for conditions such as arthritis, plantar fasciitis, and other orthopedic conditions, thereby improving clinical outcomes. For example, podiatrists can compare a patient's foot structure and movement patterns to identify potential issues, such as overpronation, and create personalized treatment plans, like targeted exercises to strengthen specific muscles or custom orthotics.

Respect to footwear designers and orthopedists, with precise data on foot rotations and moments, can create footwear and orthopedic devices that better fit the individual needs of users, providing better support and comfort. Finally, the collected data can help researchers better understand the biomechanics of the foot during specific activities such as walking, running, or jumping. This can lead to improvements in the prevention and treatment of foot-related injuries and the optimization of sports performance.

One of the main limitations of the study is having neglected the ground reaction forces in the horizontal plane, due to friction, which could slightly affect joint moments[47]. Additionally, it should be acknowledged that pressure sensors, used in this study, are less accurate than force plates for measuring ground reaction forces. Other limitations concern the experimental sample, as the inclusion criteria limited participants to men with highly supinated, normal, and highly pronated FPI. In the event of conducting a statistical analysis, the impact of unbalanced group sizes on the statistical tests should be carefully considered. Another limitation is that the data presented was obtained using the relaxed position of calcaneal standing as the reference posture, which removes the anatomical position of the foot. Therefore, anatomical offsets need to be kept in mind when analyzing extreme joint angles. However, the reference posture does not affect the joint moment data. Additionally, while our database offers valuable insights, integrating data from other relevant databases could enhance its utility. Specifically, incorporating Foot Posture Index (FPI) data into existing databases could provide a more comprehensive analysis of foot posture and biomechanics. Future updates to our database should consider including female participants and also considering a wider range of FPI variations to improve its applicability and robustness. In-shoe data would indeed be valuable; however, it would necessitate the use of alternative kinematic models[22]. Incorporating such models, along with controlled conditions[15], would be highly beneficial for the development of corrective footwear and custom insoles. Extending the analysis to the entire lower extremity —and even whole-body dynamics—would provide a more comprehensive understanding.

Code availability

The custom MATLAB code developed for calculating 3-D joint angles and moments is available at Zenodo open repository[48].

References

1. Dunn, J. E. *et al.* Prevalence of Food and Ankle Conditions in a Multiethnic Community Sample of Older Adults. *Am J Epidemiol.* **159**(5), 491–498 (2004).
2. Kuo, A. D. & Donelan, J. M. Dynamic principles of gait and their clinical implications. *Phys Ther.* **90**(2), 157–174 (2010).
3. Moreira, L., Figueiredo, J., Fonseca, P., Vilas-Boas, J. P., Santos, C. P. Lower limb kinematic, kinetic, and EMG data from young healthy humans during walking at controlled speeds. https://doi.org/10.1038/s41597-021-00881-3
4. Schulte, R. V. *et al.* Database of lower limb kinematics and electromyography during gait-related activities in able-bodied subjects. *Sci Data.* **10**(1), https://doi.org/10.1038/s41597-023-02341-6 (2023).
5. García-de-Villa, S. *et al.* A database with frailty, functional and inertial gait metrics for the research of fall causes in older adults. *Sci Data* **10**(1), 1–13, https://doi.org/10.1038/s41597-023-02428-0 (2023).
6. Lencioni T, Carpinella I, Rabuffetti M, Marzegan A, Ferrarin M. Human kinematic, kinetic and EMG data during different walking and stair ascending and descending tasks. *Sci Data.* **6**(1), 1–10, https://doi.org/10.1038/s41597-019-0323-z (2019).
7. Losing, V. & Hasenjäger, M. A Multi-Modal Gait Database of Natural Everyday-Walk in an Urban Environment. *Sci Data* **9**(1), 1–12, https://doi.org/10.1038/s41597-022-01580-3 (2022).
8. Riglet, L. *et al.* 3D motion analysis dataset of healthy young adult volunteers walking and running on overground and treadmill. *Sci Data.* **11**(1), 1–11, https://doi.org/10.1038/s41597-024-03420-y (2024).
9. Wiles, T. M. *et al.* NONAN GaitPrint: An IMU gait database of healthy young adults. *Sci Data.* **10**(1), 1–17, https://doi.org/10.1038/s41597-023-02704-z (2023).
10. Sanchis-Sales E, Sancho-Bru JL, Roda-Sales A, Pascual-Huerta J. 3D characterisation of the dynamics of foot joints of adults during walking. Gait pattern identification. *Comput Methods Biomech Biomed Engin.* **20**(9), https://doi.org/10.1080/10255842.2017.1331343 (2017).
11. Kim, E. J. *et al.* Inter-segmental foot kinematics during gait in elderly females according to the severity of hallux valgus. *J Orthop Res.* **38**(11), 2409–2418, https://doi.org/10.1002/JOR.24657 (2020).
12. Pazhooman, H., Alamri, M. S., Pomeroy, R. L. & Cobb, S. C. Foot kinematics in runners with plantar heel pain during running gait. *Gait Posture.* **104**, 15–21, https://doi.org/10.1016/J.GAITPOST.2023.05.019 (2023).
13. Chang, R., Rodrigues, P. A., Van Emmerik, R. E. A. & Hamill, J. Multi-segment foot kinematics and ground reaction forces during gait of individuals with plantar fasciitis. *J Biomech.* **47**(11), 2571–2577, https://doi.org/10.1016/J.JBIOMECH.2014.06.003 (2014).
14. Cobb, S. C., Tis, L. L., Johnson, J. T., Wang, Y. T. & Geil, M. D. Custom-molded foot-orthosis intervention and multisegment medial foot kinematics during walking. *J Athl Train.* **46**(4), 358–365, https://doi.org/10.4085/1062-6050-46.4.358 (2011).
15. Magalhães, F. A. *et al.* Clinical and biomechanical characteristics of responders and non-responders to insoles in individuals with excessive foot pronation during walking. *J Biomech.* **171**(June), https://doi.org/10.1016/j.jbiomech.2024.112182 (2024).
16. Sanchis-Sales, E., Sancho-Bru, J. L., Roda-Sales, A., Pascual-Huerta, J. Effect of static foot posture on the dynamic stiffness of foot joints during walking. *Gait Posture.* **62**, https://doi.org/10.1016/j.gaitpost.2018.03.028 (2018).
17. Bruening, D. A., Cooney, K. M. & Buczek, F. L. Analysis of a kinetic multi-segment foot model part II: Kinetics and clinical implications. *Gait Posture.* **35**(4), 535–540 (2012).
18. Gomes, R. B. O. *et al.* Foot pronation during walking is associated to the mechanical resistance of the midfoot joint complex. *Gait Posture.* **70**(August 2018), 20–23, https://doi.org/10.1016/j.gaitpost.2019.01.027 (2019).
19. Stebbins, J., Harrington, M., Thompson, N., Zavatsky, A. & Theologis, T. Repeatability of a model for measuring multi-segment foot kinematics in children. *Gait Posture.* **23**(4), 401–410 (2006).
20. Legault-Moore, D., Chester, V. L. & de Vries, G. Multisegment foot kinematics during walking in younger and older adults. *J Clin Med Res.* **4**(4), 259–266 (2012).
21. Bruening, D. A., Cooney, K. M. & Buczek, F. L. Analysis of a kinetic multi-segment foot model. Part I: Model repeatability and kinematic validity. *Gait Posture.* **35**(4), 529–534 (2012).
22. Teixeira, B. G. *et al.* Comparison between the Rizzoli and Oxford foot models with independent and clustered tracking markers. *Gait Posture.* **91**(October 2021), 48–51, https://doi.org/10.1016/j.gaitpost.2021.10.001 (2022).
23. Magalhães, F. A. *et al.* Comparison of the rigidity and forefoot – Rearfoot kinematics from three forefoot tracking marker clusters during walking and weight-bearing foot pronation-supination. *J Biomech.* **98**, 1–7, https://doi.org/10.1016/j.jbiomech.2019.109381 (2020).
24. Sanchis-Sales, E., Sancho-Bru, J. L. J. L., Roda-Sales, A. & Pascual-Huerta, J. Dynamic Flexion Stiffness of Foot Joints During Walking. *J Am Podiatr Med Assoc.* **106**(1), 37–46, https://doi.org/10.7547/14-141 (2016).
25. Redmond, A. C., Crosbie, J. & Ouvrier, R. A. Development and validation of a novel rating system for scoring standing foot posture: The Foot Posture Index. *Clin Biomech.* **21**(1), 89–98, https://doi.org/10.1016/j.clinbiomech.2005.08.002 (2006).
26. Neal, B. S. *et al.* Foot posture as a risk factor for lower limb overuse injury: a systematic review and meta-analysis. https://doi.org/10.1186/s13047-014-0055-4
27. Menz, H. B., Morris, M. E. & Lord, S. R. Foot and ankle risk factors for falls in older people: a prospective study. *J Gerontol A Biol Sci Med Sci.* **61**(8), 866–870, https://doi.org/10.1093/GERONA/61.8.866 (2006).
28. Nubé, V. L., Molyneaux, L. & Yue, D. K. Biomechanical risk factors associated with neuropathic ulceration of the hallux in people with diabetes mellitus. *J Am Podiatr Med Assoc.* **96**(3), 189–197 (2006).
29. Wu, G. *et al.* ISB recommendation on definitions of joint coordinate system of various joints for the reporting of human joint motion—part I: ankle, hip, and spine. *J Biomech.* **35**(4), 543–548, https://doi.org/10.1016/S0021-9290(01)00222-6 (2002).
30. Faul, F., Erdfelder, E., Lang, A.-G. & Buchner, A. G. *Power 3: A flexible statistical power analysis program for the social, behavioral, and biomedical sciences. *Behav Res Methods.* **39**(2), 175–191, https://doi.org/10.3758/BF03193146 (2007).
31. Cohen J. *Statistical Power Analysis for the Behavioral Sciences.* 2nd ed. Lawrence Erlbaum Associates; https://doi.org/10.1016/B978-0-12-179060-8.50017-7 (1988).
32. Sanchis-Sales, E., Sancho-Bru, J. L. J. L., Roda-Sales, A. & Pascual-Huerta, J. Variability of the dynamic stiffness of foot joints: Effect of gait speed. *J Am Podiatr Med Assoc.* **109**(4), 291–298, https://doi.org/10.7547/17-035 (2019).
33. Söderkvist, I. & Wedin, P. A. Determining the movements of the skeleton using well-configured markers. *J Biomech.* **26**(12), 1473–1477 (1993).
34. Sancho-Bru, J. L., Sanchis-Sales, E., Rodríguez-Cervantes, P. J., Vergés-Salas, C. Foot Sole Contact Forces vs. Ground Contact Forces to Obtain Foot Joint Moments for In-Shoe Gait—A Preliminary Study. *Sensors (Basel).* **23**(15), https://doi.org/10.3390/S23156744 (2023).
35. Crenna, P. & Frigo, C. Dynamics of the ankle joint analyzed through moment–angle loops during human walking: Gender and age effects. *Hum Mov Sci.* **30**(6), 1185–1198 (2011).

36. Shamaei, K., Sawicki, G. S. & Dollar, A. M. Estimation of quasi-stiffness of the human hip in the stance phase of walking. *PLoS One.* **8**(12), e81841 (2013).
37. Davis, R. B. & DeLuca, P. A. Gait characterization via dynamic joint stiffness. *Gait Posture.* **4**(3), 224–231 (1996).
38. Sanchis-Sales, E., Sancho-Bru, J. L., Roda-Sales, A., Chiva-Miralles, M. J., García-Gomáriz, C. Foot kinematics and kinetics data for different static foot posture collected using a multi-segment foot model. Zenodo. https://doi.org/10.5281/zenodo.10838066 (2024).
39. Saraswat, P., MacWilliams, B. A., Davis, R. B. & D'Astous, J. L. Kinematics and kinetics of normal and planovalgus feet during walking. *Gait Posture.* **39**(1), 339–345 (2014).
40. Buldt, A. K. *et al.* Foot posture is associated with kinematics of the foot during gait: A comparison of normal, planus and cavus feet. *Gait Posture.* **42**(1), 42–48 (2015).
41. Magalhães, F. A. *et al.* Midfoot passive stiffness affects foot and ankle kinematics and kinetics during the propulsive phase of walking. *J Biomech.* **119**. https://doi.org/10.1016/J.JBIOMECH.2021.110328 (2021).
42. Kern, A. M., Papachatzis, N., Patterson, J. M., Bruening, D. A. & Takahashi, K. Z. Ankle and midtarsal joint quasi-stiffness during walking with added mass. *PeerJ.* **7**(9). https://doi.org/10.7717/PEERJ.7487 (2019).
43. Bruening, D. A. & Takahashi, K. Z. Partitioning ground reaction forces for multi-segment foot joint kinetics. *Gait Posture.* **62**, 111–116, https://doi.org/10.1016/J.GAITPOST.2018.03.001 (2018).
44. Kruger, K. M. *et al.* Segmental foot and ankle kinematic differences between rectus, planus, and cavus foot types. *J Biomech.* **94**, 180–186, https://doi.org/10.1016/J.JBIOMECH.2019.07.032 (2019).
45. Matsumoto, Y. *et al.* Novel Multi-Segment Foot Model Incorporating Plantar Aponeurosis for Detailed Kinematic and Kinetic Analyses of the Foot With Application to Gait Studies. *Article.* **10**, 1, https://doi.org/10.3389/fbioe.2022.894731 (2022).
46. Buldt, A. K., Allan, J. J., Landorf, K. B. & Menz, H. B. The relationship between foot posture and plantar pressure during walking in adults: A systematic review. *Gait Posture.* **62**(February), 56–67, https://doi.org/10.1016/j.gaitpost.2018.02.026 (2018).
47. Hunt, A. E., Smith, R. M. & Torode, M. Extrinsic muscle activity, foot motion and ankle joint moments during the stance phase of walking. *Foot ankle Int.* **22**(1), 31–41, https://doi.org/10.1177/107110070102200105 (2001).
48. Roda-Sales, A., Sancho-Bru, J. L., Sanchis-Sales, E. StiffnessAnalysis: Calculation code of foot kinematics and kinetics using a multi-segment foot model. Zenodo https://zenodo.org/doi/10.5281/zenodo.10890093 (2024).
49. Ogawa, R. & Hyakusoku, H. Does Egyptian foot present an increased risk of ingrown toenail? *Plast Reconstr Surg.* **117**(6), 2111–2112, https://doi.org/10.1097/01.PRS.0000214750.33936.45 (2006).

Author contributions
E.S.-S. created the experimental protocol, acquired data, performed data analysis and wrote the paper. J.L.S.-B. conceived and planned the project, conducted and supervised the experiment and wrote the paper and revised the data structure. A.R.-S. developed the Matlab code to calculate joint angles and moments, wrote the paper and created the data structure. M.J. C.-M. acquired data and reviewed the paper. C.G.-G. acquired data and reviewed the paper. All authors have read and agreed to the published version of the manuscript.

Competing interests
The authors declare no competing interests.

Additional information
Correspondence and requests for materials should be addressed to E.S.-S.

Reprints and permissions information is available at www.nature.com/reprints.

Publisher's note Springer Nature remains neutral with regard to jurisdictional claims in published maps and institutional affiliations.